Advances in Reliability, Safety and Security, Part 6 – Kołowrocki, Magryta-Mut (eds.)

Advances in Reliability, Safety and Security

ESREL 2024
Monograph Book Series

Predictive Maintenance Planning For Batteries Of Electric Take-Off And Landing (eVTOL) Aircraft Using State-of-Health Prognostics

Mihaela Mitici[a], Leo Jenneskens[a], Zhiguo Zeng[b], David Coit[b]

[a]*Utrecht University, Utrecht, the Netherlands*
[b]*Central Supelec Universite Paris-Saclay, Paris, France*
[c]*Rutgers University, New Jersey, USA*

Abstract

Electric vertical take-off and landing (eVTOL) aircraft are a futuristic, sustainable transportation mode aimed at reducing traffic congestion. The health management of eVTOL batteries is key for the deployment of such aircraft. In this paper, we consider the continuous monitoring of eVTOL batteries, with streams of measurements related to the charging, discharging, and temperature of the batteries. Based on these measurements, we develop a Convolution Neural Network with Monte Carlo dropout to estimate the distribution of the State-of-Health (SOH) of the batteries, i.e., we develop probabilistic SOH prognostics. The features used for the SOH estimates are selected based on the feature importance quantified by Shapley values. The obtained probabilistic SOH prognostics are further employed for the maintenance planning of the eVTOL batteries. The results show that our approach leads to accurate SOH estimates. Moreover, we are able to identify optimal times for eVTOL battery replacement, as a trade-off between the cost of unexpected failure and the cost of wasted battery life.

Keywords: predictive maintenance, batteries, State-of-Health, prognostics, electric take-off and landing aircraft, eVTOL

1. Introduction

Urban mobility needs, together with traffic congestion, are expected to increase in the coming years. To address this, electric short-range aircraft such as electric Vertical Take-off and Landing (eVTOL) aircraft are seen as a promising solution. Existing eVTOL designs achieve average ranges of 50-100km, at an average speed of 200km/hr, having a payload of up to 500-800kg (Polaczyk, Enzo, Wei, & Mitici, 2019). The most frequently considered battery technology for current eVTOLs is lithium-ion due to its high energy density, low self-discharge rates and feasible costs (Mitici, Hennink, Pavel, & Dong, 2023). Battery management, however, is one of the main challenges for EVTOL operations. In particular, the continuous monitoring of the state-of-health of the battery is a priority for safe and efficient eVTOL operations.

Several studies have focused on lithium-ion battery management for on-ground vehicles, with a focus on estimating the State-of-Health (SOH) and the Remaining-Useful-Life (RUL) of the batteries (Tian, Qin, Li, & Zhao, 2020). Different from the operations of electric ground vehicles, the take-off and landing are critical phases of an eVTOL flight, with larger battery discharge rates compared to the cruise phase. In the long-run, this is expected to have a direct impact on the SOH of the batteries. In this paper, we analyze the SOH of eVTOL batteries by distinguishing the use of the battery at different stages of the flight – take-off, cruise, and landing.

For SOH estimation of lithium-ion batteries, many recent studies consider data-driven machine learning approaches. In (Mawonou, Eddah, Dumur, Beauvois, & Godoy, 2021), the SOH of batteries of automotives is estimated using random forest together with two aging indicators, which consider the distance, speed, temperature, and charging power of the automotives. In (Liu, Zhao, Wang, & Yang, 2020), a support vector regression is proposed, which is based on dynamic health indicators extracted from the battery charging curves. A random forest

regression is proposed in (Li, et al., 2018) based on directly measured signals such as current and voltage. The authors develop online, accurate estimates for the SOH with a root-mean-square error of less than 1.3%.

All studies above, however, consider batteries that are envisioned for ground operations, with constant CC and CV cycling. For electric vertical take-off and landing (eVTOL) aircraft, the characteristics of the flight and particularly the critical take-off and landing phases of a flight, pose additional challenges for the health management of the eVTOL batteries, compared to batteries for ground operations. To the best of our knowledge, the dataset in (Bills, et al., 2023) is the first to consider the health monitoring of eVTOL batteries. This dataset includes distinct eVTOL mission profiles and battery measurements specified for the take-off, cruise, and landing phase of the flights. In particular, the batteries are subject to different C-rates during the discharge phase of a flight, with the take-off and landing of eVTOLs being performed at a larger C-rate than during the cruise phase. Moreover, the batteries undergo various flight conditions across flight missions, with the temperature, power during discharge, and cruise length being varied across multiple missions. Only a few, recent studies have developed SOH and/or RUL prognostics for the eVTOL batteries using the dataset (Bills, et al., 2023). In (Granado, Ben-Marzouk, Saenz, Boukal, & Juge, 2022), the authors develop SOH estimates for the batteries using linear regression, support vector machines (SVM), k-nearest neighbors (kNN), random forest (RF) and light gradient boosting machine (LGBM), with the kNN outperforming the other four algorithms. However, (Granado, Ben-Marzouk, Saenz, Boukal, & Juge, 2022) considers only the measurements recorded during the cruise phase of the flight, which is a strong limitation since the vertical climb and descent are the most critical phases for the battery life of eVTOLs. In (Mitici, Hennink, Pavel, & Dong, 2023), the authors consider all the flight phases (take-off, cruise, landing) and develop machine learning models for both SOH and RUL prognostics. The results show that the features with the highest importance for SOH estimation are the (variance, minimum) voltage recorded during take-off and the duration of the CC-CV charging phase. As such, the authors show the importance of discriminating features based on the flight phases of the eVTOLs. Accurate SOH prognostics are achieved by employing a Random Forrest Regression with a 5-fold cross validation. Similar to (Mitici, Hennink, Pavel, & Dong, 2023), in this paper we also consider all phases of the flight (take-off, cruise, landing) and discriminate between these phases when constructing features for SOH prognostics. Different from existing studies on health prognostics of eVTOL batteries, however, in this paper we estimate the distribution of the SOH, i.e., we obtain *probabilistic* SOH prognostics, rather than generating point estimated of the SOH. Moreover, we further employ these probabilistic SOH prognostics for the maintenance planning of the batteries.

In this paper we propose a framework for probabilistic SOH prognostics and predictive maintenance planning of eVTOL batteries. We generate features based on variables related to the charge/discharge protocols, the temperature at which batteries are exposed, the flight phases of the eVTOLs and original voltage-capacity/time curves. We consider an End-of-Life (EOL) for the eVTOL batteries of 85% of the battery capacity, rather than 80% as it is commonly assumed for on-ground electric vehicles. This is due to the rapid degradation of the batteries in the case of eVTOLs. We estimate the distribution of the SOH of the batteries using a Convolutional Neural Network with Monte Carlo dropout. These prognostics are re-generated/updated periodically, after every capacity test, as more measurements become available. The results show that our approach approximates well the distribution of the SOH, with the Continuous Ranking Probability Score (CRPS) indicating a well centered distribution around the true SOH. We further employ the obtained distribution of the SOH to determine an optimal replacement time for the batteries, taking into account the high cost of a battery being inoperable as it reaches its EOL, and the cost of early battery replacement or, equivalently, the cost of wasting the life of the battery. Overall, we provide an end-to-end predictive maintenance planning for eVTOL batteries, taking into account the ongoing monitoring of the health state of these batteries.

This paper is organized as follows. In Section 2 we introduce the eVTOL battery dataset and formalize the eVTOL mission profiles. In Section 3 we develop features for SOH estimation based on the measurement available, and quantity the importance of these features by determining their Shapley value. We further develop a Convolutional Neural Network with Monte Carlo dropout to obtain probabilistic SOH prognostics. In Section 4 we introduce a maintenance planning framework for battery replacement, based on the probabilistic SOH prognostics obtained. Lastly, Section 5 provides the conclusions of this study.

2. Data description

We consider the condition-monitoring dataset for Sony-Murata 18650 VTC-6 cell lithium-ion batteries (Bills, et al., 2023). These batteries are used to perform a sequence of missions for VAHANA electric take-off and landing (eVTOL) aircraft. One battery is allocated for sequence of missions, with each of these missions following a given mission profile, i.e., a Constant Current (CC) battery Charging phase, a Constant Voltage (CV) battery Charging phase, a Rest period, a Takeoff segment at a given power, a Cruise segment at a given duration and

power, a Landing segment at a given power. In total, dataset (Bills, et al., 2023) consists of 22 distinct mission profiles (MP1-MP22), see Table 1.

Table 1: Characteristics of the mission profiles (MPs) based on (Bills, et al., 2023), with MP1, MP13 and MP20 baseline mission profiles.

	Cruise duration (sec)	Power take-off (W)	Power cruise (W)	Power landing (W)	CC	CV	Ambient temperature (°C)	VAH	# missions	# capacity tests
MP1	800	54	16	54	1C	4.2	25	VAH01	847	16
MP2	1.25*800	54	16	54	1C	4.2	25	VAH02	625	12
MP3	800	0.9*54	0.9*16	0.9*54	1C	4.2	25	VAH05	1615	29
MP4	800	54	16	54	0.5*1C	4.2	25	VAH06	9290	19
MP5	800	54	16	54	1C	0.9524*4.2	25	VAH07	339	44
MP6	800	54	16	54	1C	4.2	0.8*25	VAH09	8527	23
MP7	800	54	16	54	1C	4.2	1.2*25	VAH10	1431	27
MP8	800	0.8*54	0.8*16	0.8*54	1C	4.2	25	VAH11	2249	44
MP9	0.5*800	54	16	54	1C	4.2	25	VAH12	2349	45
MP10	0.75*800	54	16	54	1C	4.2	25	VAH13	1042	19
MP11	1.25*800	54	16	54	1C	4.2	25	VAH15	554	10
MP12	800	54	16	54	1.5*1C	4.2	25	VAH16	559	10
MP13	800	54	16	54	1C	4.2	25	VAH17	1002	19
MP14	800	54	16	54	1.5*1C	4.2	25	VAH20	611	11
MP15	1.25*800	54	16	54	1C	4.2	25	VAH22	579	10
MP16	800	54	16	54	1C	0.9762*4.2	25	VAH23	697	13
MP17	800	54	16	54	0.5*1C	4.2	25	VAH24	801	15
MP18	800	54	16	54	1C	4.2	0.8*25	VAH25	554	10
MP19	0.75*800	54	16	54	1C	4.2	25	VAH26	1164	22
MP20	800	54	16	54	1C	4.2	25	VAH27	587	11
MP21	800	0.9*54	0.9*16	0.9*54	1C	4.2	25	VAH28	1182	22
MP22	800	54	16	54	1C	4.2	1.4*25	VAH30	919	17

In Table 1, VAH01, VAH17, and VAH27, are baseline mission profiles. Starting from these baseline mission profiles, mission parameters are varied to obtain the remining mission profiles. Under a baseline mission profile, during the CC charging phase, the battery is charged at 1C rate until the battery voltage reaches 4.2V. This is followed by the CV charging phase, when a constant voltage of 4.2V is maintained until the current drops below C/30. Charging is followed by a cooling period when the battery temperature reaches 35°C. After the Rest period, a mission is performed. Under the baseline mission profile, the mission is characterized by a Take-off phase of 75sec, during which a discharge rate of 5C is observed. The cruise phase follows for a duration of 800sec. Subsequently, the landing phase lasts for 105sec during which the battery is subject to a discharge rate of 5C.
Błąd! Nie można odnaleźć źródła odwołania. shows the characteristics of the first capacity test of the battery under VAH01 mission profile. The CC charging phase has a duration of 50min, when the battery is charged with 3.0A. The CV charging phase follows for 33min with 4.2V. Next, the Rest period has a duration of 14min. The discharge phase starts as soon as the eVTOL takes-off, having a duration of 75sec. During take-off, the voltage drops from 3.92V to 3.62V. Next, the cruise phase has a duration of 800sec. Lastly, the landing phase takes 105sec, during which the voltage drops from 3.57V to 3.1V. Finally, a Rest period of 605sec follows. At the end of the Rest period, the battery reaches a temperature of 27.3°C.

Measurements - during each mission, the following measurements are recorded: time (sec), cell voltage (V), cell current (mA), energy supplied to the cell during charge (Wh), charge supplied to the cell during charge (mAh), energy extracted from the cell during discharge (Wh), charge extracted from the battery cell during discharge (mAh), cell surface temperature (°C), impedance at 20% Depth-of-Discharge (DOD) after 1 and 30 sec of low current, (°C), impedance at 60% Depth-of-Discharge (DOD) after 1 and 30 sec of low current , cycle number (-), cycle segment (-).

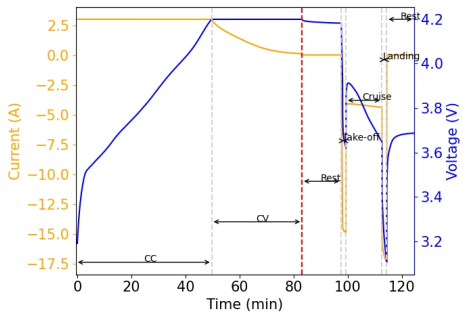

Fig. 1. Characteristics of the first capacity test of the battery under mission profile VAH01.

Capacity tests - Given a profile mission, after every 50th mission, the residual battery charge is discharged at a rate C/5 until the voltage drops below 2.5V and SOC=0%. Subsequently, a period of Rest is observed, during which the battery's temperature drops below 30°C. Following this cooling phase, the battery is charged to SOC=100% at a charging rate of 1 C-rate and a constant voltage of 4.2V. Having the battery fully charged, the battery performs the next mission, referred to as the "capacity test". Table 1 shows the total number of capacity tests under each of the 22 mission profiles. We note that the very first mission of an eVTOL is a capacity test.

To estimate the battery SOH, we consider the battery capacity during capacity tests only. We only focus on the capacity tests since dynamic capacity estimation would require an extensive analysis and hyperparameter tuning, which may be prone to estimation errors (Xiong, 2020). In contrast, a regular static capacity calibration is more reliable for testing purposes.

Data processing of mission profiles – mission profiles MP8 (VAH11), and MP19 (VAH26) have their impedance data incomplete or missing, respectively. As a result, we will not consider these two mission profiles in our analysis. Mission profiles MP4(VAH06), MP6(VAH09), MP19 (VAH26), MP20(VAH27) exhibit a decreasing capacity (mAh) across subsequent capacity tests, with a significant drop starting from capacity test 15, 11, 5, 5 respectively. This drop is observed for three consecutive capacity tests, after which the capacity unexpectedly increases significantly. Thereafter, the capacity decreases smoothly across the remaining capacity tests. To adjust for this unexpected behavior in the data, the capacity c_i corresponding to capacity tests i in the capacity dip have been smoothened as $c_i = (c_{i-1} + c_{i+1})/2$.

3. Probabilistic SOH prognostics using Convolutional Neural Networks with Monte Carlo dropout

In this section we propose a data-driven machine learning approach to estimate the distribution of the State-of-Health (SOH) of the batteries based on the measurements available across multiple missions (see Section 2). We first define the SOH of a battery. Next, we design features based on the available measurements in the dataset (Bills, et al., 2023), and select those features with the highest importance for SOH estimation. Lastly, using the selected features, we introduce a Convolutional Neural Network to estimate the distribution of the SOH of the batteries.

Let M define the set of mission profiles considered, with $|M| = 20$. Let $C^m, m \in M$ define the number of capacity tests of mission profile m. We define the SOH of the battery under mission profile $m \in M$ at capacity test $1 \leq c \leq C^m$, denoted by $SOH^{m,c}$, as follows:

$$SOH^{m,c} = \frac{Qcharge^{m,c}}{Qcharge^{m,0}} \cdot 100\%,$$

where $Qcharge^{m,c}$ is the capacity at capacity test $c \geq 1$ of mission profile m, and $Qcharge^{m,0}$ is the capacity at the first capacity test $c = 0$ of mission profile m.

3.1. Feature engineering

Following (Mitici, Hennink, Pavel, & Dong, 2023), we consider a total of 37 features. These features are related to the charging, discharging, temperature and impedance of the battery, as follows.

- *Charging-related features*

Given the impact of the duration of the CC and CV charging on the battery capacity across missions (Caiping, et al., 2017), we consider the following charging related features: the duration (sec) of the CC charging phase of capacity test c of mission m, denoted by $\Delta^{CC,m,c}$; the duration (sec) of the CV charging phase of capacity test c of mission m, denoted by $\Delta^{CV,m,c}$; the duration (sec) of the Rest period after the charging of capacity test $c, 1 \leq c \leq C_m$ of mission $m, m \in M$, denoted by $\Delta^{rest,m,c}$, with $1 \leq c \leq C_m, m \in M$.

- *Discharge-related features*

We consider features related to i) the discharge voltage of the battery, ii) the discharge capacity, and iii) the duration of the discharge during each segment of the mission (take-off, cruise, landing). Because the discharge voltage varies during the mission segments take-off, cruise, landing, as well as across capacity tests, we capture the impact of these variations by considering the as voltage-related features the maximum, minimum, mean, and the variance of the voltage during each mission segment (take-off, cruise, landing) of capacity test c of mission m, which we denote by $V_{max}^{segment,m,c}$, $V_{min}^{segment,m,c}$, $V_{mean}^{segment,m,c}$, $V_{var}^{segment,m,c}$, respectively, with $1 \leq c \leq C_m, m \in M$. The discharge capacity and its variation reflect the load characteristics of the battery. The evolution of the discharge capacity across missions is captured by the maximum, minimum, mean and the variance of the discharge capacity during each mission segment (take-off, cruise, landing) of capacity test c of mission m, which we denote by $Qdis_{max}^{segment,m,c}$, $Qdis_{min}^{segment,m,c}$, $Qdis_{mean}^{segment,m,c}$, $Qdis_{var}^{segment,m,c}$ respectively, with $1 \leq c \leq C_m, m \in M$. Lastly, we consider the duration of the discharge during each mission segment, denoted by $\Delta^{segment,m,c}$, $1 \leq c \leq C_m, m \in M$.

- *Temperature-related features*

For all batteries in the dataset, it holds that as the battery ages, the temperature of the battery tends to increase. To capture the battery temperature across missions, we consider the maximum temperature reached during each mission segment (take-off, cruise, landing), denoted by $T_{max}^{segment,m,c}$ with $1 \leq c \leq C_m, m \in M$.

- *Impedance-based features*

Additionally to the measurements, we consider the calculated impedance at 20% Depth of-Discharge (DOD) after 1 sec and after 30 sec of low current, denoted by $I^{20\%,1,m}$, $I^{20\%,30,m}$ respectively, and the impedance at 60% Depth of-Discharge (DOD) after 1 sec and after 30 sec of low current, denoted by $I^{60\%,1,m}$, $I^{60\%,30,m}$ respectively, during each mission $m \in M$.

3.2. Feature importance quantification and feature selection

In Section 3.1 a total of 37 features have been considered. In this section we quantify the importance of these features for SOH estimation using the Shapley additive explanations (SHAP) values (Lundberg & Lee, 2017), which determine the impact of a feature on the SOH estimation. We determine the SHAP value as follows:

$$\sum_{S \subseteq F\{i\}} \frac{|S|!(|F|-|S|-1)!}{|F|!} [f(S \cup \{i\}) - f(S)],$$

where F is the set of all features considered for the SOH estimation algorithm, $S \subseteq F\{i\}$ is a subset of features obtained from the set F except feature i, and $f(S)$ is the expected algorithm output given by the set S of considered features. The SHAP value quantifies the magnitude of the impact, i.e., how much a specific feature value contributes to the accurate estimation of the SOH, where a large SHAP value for a given feature indicates a large importance of this feature for the SOH estimation.

Błąd! Nie można odnaleźć źródła odwołania. shows the SHAP values obtained for the 37 features considered. Based on the SHAP values, we select the top 65% features with the highest SHAP value (importance), leading to a total of 24 selected features for SOH estimation. The results show that the variance of the voltage during take-off, $V_{var}^{take-off}$, which increases as the SOH decreases, has the highest importance. The CC and CV charging durations, Δ^{CC} and Δ^{CV}, also exhibit a high importance, followed by the minimum voltage during take-off, $V_{min}^{take-off}$, and the impedance at 60% DOD, $I^{60\%}$, and the maximum voltage during the cruise segment, $V_{max}^{take-off}$. As expected, the features related to the take-off segment have a high importance since the battery experiences a high discharge voltage during take-off. Due to the high discharge voltages, the internal resistance increases. This, in turn, impacts the SOH of the battery (Huang, Tseng, Liang, Chang, & Pecht, 2017). Also, the high importance

of the duration of the CC charging phase is expected, since, as the number of missions performed by the batteries increases, the SOH decreases while the duration of the CC charging phase increases.

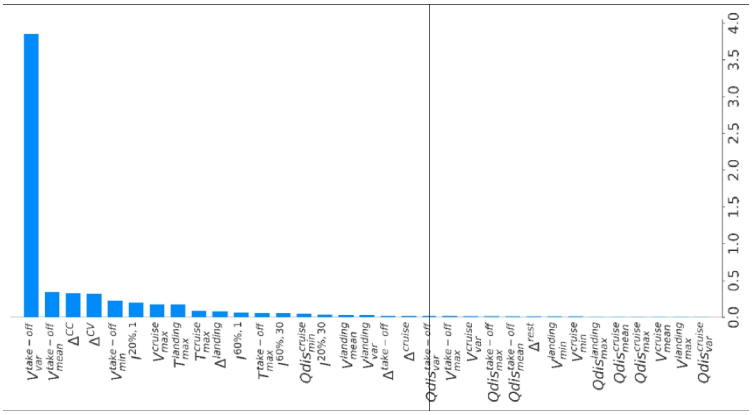

Fig. 2. SHAP values - feature importance.

3.3. Convolutional Neural Network with Monte Carlo dropout for probabilistic SOH prognostics

The CNN has L convolutional layers, with each layer consists of K filters. Each kernel has a size of $1\times S$, i.e., one-dimensional kernels. The convolutional operation in the lth convolutional layer for the nth filter k_n^l is (Wang, Lei, Li, & Yan, 2019):

$z_n^l = \tanh(k_n^l * z^{l-1} + b_n^l)$,

where z_n^l is the nth feature map of layer l, $*$ is the convolutional operator, z^{l-1} are the feature maps in layer $l-1$, b_n^l is the bias of the nth filter of layer l, and $\tanh(.)$ denotes the hyperbolic tangent activation function. We then consider a single convolutional layer with one filter, where each kernel has a size of $1 \times S'$. This layer combines all K feature maps in one single feature map. Let z^L denote the output of this last convolutional layer.

Finally, we add two fully connected layers which predict the RUL based on the extracted features of the last convolutional layer. The output z^f of the first fully connected layer is (Wang, Lei, Li, & Yan, 2019):

$z^f = \tanh(w^f z^L + b^f)$,

where b^f is the bias and w^f are the weights of the first fully connected layer. A second fully connected layer with one neuron and the ReLU activation function outputs the SOH prediction, where the ReLU activation function has an upper and a lower bound to ensure that $0\% \leq SOH \leq 100\%$.

Monte Carlo dropout

Commonly, Monte Carlo dropout is applied in the training phase of the neural networks to avoid overfitting. To obtain the distribution of the SOH, i.e., to obtain probabilistic SOH prognostics, we also apply Monte Carlo dropout in the testing phase

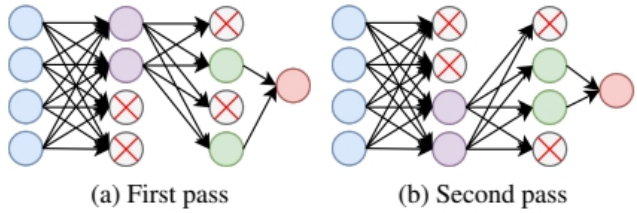

Fig. 3. Illustrative example of a neural network with Monte Carlo dropout, during two passes of a sample through a network.

of the CNN (Gal & Ghahramani, 2016). In this line, (Gal & Ghahramani, 2016) shows that such a neural network with Monte Carlo dropout approximates a Bayesian neural network representing a deep Gaussian process.

We consider a dropout rate $\rho = 30\%$ in each layer of the CNN, except the first layer so that we avoid the loss of input information. We perform 1.000 forward passes through the network for each test sample. During the pass, a ρ fraction of the neurons are dropped, which generates a potentially different SOH estimate. Considering all

passes, we obtain a distribution of the SOH estimate. **Błąd! Nie można odnaleźć źródła odwołania.** shows an illustrative example of a neural network with Monte Carlo dropout with two passes.

3.4. Performance metrics

Using CNN with Monte Carlo dropout, we estimate the distribution of the SOH of the batteries for all 20 mission profiles considered and at each capacity test. We evaluate the performance of your SOH estimates using the Mean Absolute Error (MAE), the Root Mean Squared Error ($RMSE$), the Continuous Ranking Probability Score ($CRPS$), which assesses the estimation performance of the probabilistic RUL prognostics, and the Weighted Continuous Ranking Probability Score ($CRPS^W$) (de Pater & Mitici, 2022), which penalizes the over/underestimation of the RUL as follows:

$MAE = \frac{1}{M}\sum_{j=1}^{M} MAE^j$, with $MAE^m = \frac{1}{C^m}\sum_{i=1}^{C^m} SOH^{m,i} - \widehat{SOH^{m,i}}$;

$RMSE = \frac{1}{M}\sum_{j=1}^{M} RMSE^j$, with $RMSE^m = \sqrt{\frac{1}{C^m}\sum_{i=1}^{C^m}(SOH^{m,i} - \widehat{SOH^{m,i}})^2}$;

$CRPS^m = \frac{1}{C^m}\sum_{i=1}^{C^m} CRPS^{m,i}$, with $CRPS^{m,i} = \int_{-\infty}^{\infty}\left[F_{\hat{y}_{m,i}}(x) - I(y_{m,i} \le x)\right]^2 dx$, $I(y_{m,i} < x)\begin{cases}1, y_{m,i} < x\\ 0, y_{m,i} > x\end{cases}$;

$CRPS^{W,m} = \frac{1}{C^m}\sum_{i=1}^{C^m} CRPS^{W,m,i}$, with $CRPS^{W,m,i} = (2-\beta)\int_{-\infty}^{y_{m,i}}\left(F_{\hat{y}_{m,i}}(x)\right)^2 dx + \beta\int_{y_{m,i}}^{\infty}[F_{\hat{y}_{m,i}}(x) - 1]^2\, dx$,

where $SOH^{m,i}$ is the true battery SOH at capacity test i of mission profile m, $\widehat{SOH^{m,i}}$ is the mean of the predicted distribution of SOH at capacity test i of mission profile $m \in M$, $F_{\hat{y}_{m,i}}(x)$ is the estimated, empirical CDF of the RUL at capacity test i of mission profile m, and β an user-defined penalty parameter for the RUL being overestimated/underestimated, with $0 \le \beta \le 2$. The smaller the CRPS metric is, the closer the RUL estimate is to the actual RUL. For a perfect RUL prediction, $CRPS = 0$ and $CRPS^W = 0$.

3.5. Numerical results – Probabilistic SOH prognostics of eVTOL batteries

We illustrate our RUL estimation methodology for the selected 20 batteries and their mission profiles, using a leave-one-out approach, i.e., we consider 20 experiments, choosing a different battery for testing in each experiment, while the remaining 19 batteries are used in the training phase. We update the SOH prognostics periodically, after every capacity test, as more measurements become available.

Table 2: Performance evaluation of the CNN with Monte Carlo dropout for SOH estimation. shows the performance of the CNN with Monte Carlo dropout for SOH estimation. The results show that the SOH is estimated well for all VAH, with the lowest MAE of 0.51% for VAH17 and the highest MAE of 2.65% for VAH30. Most importantly, the distribution of the SOH is also accurately estimated, with the lowest CRPS of 0.38 for VAH17 and VAH24, while the highest CRPS is 2.35 for VAH30. Also, for those batteries when $CRPS^W < CRPS$, the results show that SOH is relatively often underestimated. In the other cases, the SOH is overestimated. When considering all batteries, the results show that the CNN relatively often underestimates the actual SOH.

Błąd! Nie można odnaleźć źródła odwołania. shows an example of the estimate distribution of the SOH for VAH09 at the 1st and 9th capacity test. The true SOH is given in the red, vertical line, while the green vertical line is the average of the estimated distribution.

Table 2: Performance evaluation of the CNN with Monte Carlo dropout for SOH estimation.

VAH#	MAE	$RMSE$	$CRPS$	$CRPS^W$
VAH01	1.30	1.73	1.03	0.61
VAH02	1.77	1.89	1.51	0.94
VAH05	1.72	1.95	1.42	2.07
VAH06	1.48	2.20	1.22	0.70
VAH07	1.48	1.71	1.11	1.67
VAH09	0.98	1.15	0.75	1.12
VAH10	1.36	1.75	1.10	1.18
VAH12	1.61	1.89	1.35	1.46
VAH13	1.90	2.19	1.69	2.52
VAH15	0.88	0.95	0.69	0.36
VAH16	1.01	1.08	0.81	0.41
VAH17	0.51	0.63	0.38	0.36
VAH20	1.08	1.46	0.91	1.13
VAH22	2.05	2.43	1.75	0.87
VAH23	2.51	2.74	2.28	2.76
VAH24	0.48	0.66	0.38	0.23
VAH25	0.81	0.92	0.64	0.43
VAH27	0.70	0.90	0.56	0.60
VAH28	0.81	0.99	0.61	0.44
VAH30	2.65	2.95	2.35	3.49
ALL	1.35	1.61	1.15	1.25

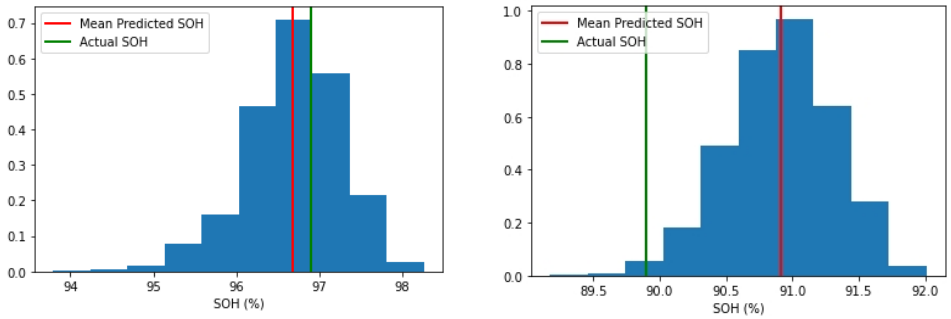

Fig. 4. The estimated distribution of the SOH for VAH09, at the 1st (left figure) and 9th (right figure) capacity test.

4. Predictive maintenance planning for eVTOL batteries integrating probabilistic SOH prognostics

4.1. Modelling the maintenance planning of batteries by integrating probabilistic SOH prognostics

We consider the case of having estimates of the distribution of the battery SOH at the end of every mission (cycle). Based on these estimates, at the end of every cycle we are interested in determining whether the battery should be replaced or whether this decision should be postponed for the next mission. We assume that a too early replacement is costly due to the wasted life of the battery, and due to maintenance costs for battery replacement. At the same time, an unscheduled battery replacement due to an inoperable battery is very costly, and possess safety risks. We say that a battery is *inoperable* if the SOH of this battery is below a threshold $T > 0$.

Most existing studies define the End-of-Life (EOL) of batteries as the first moment the capacity of the battery is below a threshold of 80% of the nominal battery capacity (Severson, et al., 2019), (Yang, Wang, Xu, Huang, & Tsui, 2020), (Zhang, Xiong, He, & Pecht, 2018), i.e., $T = 0.8$. To the best of our knowledge, thresholds for the EOL of eVTOL batteries have not been formally established. Compared to batteries for automotives, we expect

that more conservative safety margins will be applied for eVTOL batteries. In preliminary studies on eVTOL batteries such as (Alba-Maestre, Prud'homme van Reine, Sinnige, & Castro, 2021), (Mitici, Hennink, Pavel, & Dong, 2023) a conservative EOL threshold of 85% of a nominal battery capacity has been considered. Following (Alba-Maestre, Prud'homme van Reine, Sinnige, & Castro, 2021) (Mitici, Hennink, Pavel, & Dong, 2023), in this paper we also consider an EOL threshold of $T = 85\%$ of the initially measured battery capacity. Even so, VAH07 and VAH23 do not reach the threshold of $T = 85\%$ even at the end of their last missions. Due to this reason, we do not consider VAH07 and VAH23 for maintenance planning.

For battery replacement planning, given a current capacity test c, we consider the following costs. In case the decision is to replace the battery at the end of current capacity test c, then a cost $c_{scheduled}$ for a preventive, scheduled battery replacement is incurred, where

$$c_{scheduled} = \frac{c_0}{c},$$

with c_0 a fixed cost of battery replacement, $c_0 > 0$. Here, early scheduled battery replacements (wasted life of the battery) lead to high maintenance costs. Otherwise, the decision to replace the battery is postponed for the next capacity test, with an associated cost of having to perform an unscheduled battery replacement due to this battery being inoperable, i.e., we assume the following cost for corrective maintenance:

$$c_{corrective} = \frac{c_{unscheduled} \cdot P(SOH_c \leq T)}{c+1},$$

with $c_{unscheduled}$ the cost of performing an unscheduled replacement, and $P(SOH_c \leq T)$ the probability that the SOH estimated at capacity test c (using the approach in Section 3) is below an EOL threshold T, where $T = 0.85$. Here, $P(SOH_c \leq T)$ quantifies the risk of having an inoperable battery in the upcoming capacity test. We assume that $c_{unscheduled} \gg c_{scheduled}$. By evaluating $c_{scheduled}$ and $c_{corrective}$ at the end of capacity test c, a decision is made of whether to replace the battery or postpose the decision for next mission.

4.2. Numerical results – maintenance planning of eVTOL batteries integrating probabilistic SOH prognostics

Table 3: Maintenance planning for eVTOL batteries, where c^N is the last capacity test when the decision is Not to replace the battery, $p_{c^N}^{SOH} = P(SOH_{c^N} \leq 0.85)$, i.e., the estimated probability at capacity test c^N that the SOH of the battery is below the threshold $T = 0.85$, c^R is the first capacity test when the decision is to Replace the battery, $p_{c^R}^{SOH} = P(SOH_{c^R} \leq 0.85)$, i.e., the estimated probability at capacity test c^R that the SOH of the battery is below the threshold $T = 0.85$. shows an optimal moment (capacity tests) to replace the battery, based on the estimated distribution of the SOH at the capacity tests. Here, we consider a cost for battery replacement $c_0 = 10$ and a cost $c_{unscheduled} = 100$ for an unscheduled battery replacement. The results show a switch in the estimated $P(SOH_c \leq 0.85)$ between the last capacity test c^N when no battery replacement is planned, and the first capacity test c^R when a battery replacements is recommended.

Table 3: Maintenance planning for eVTOL batteries, where c^N is the last capacity test when the decision is Not to replace the battery, $p_{c^N}^{SOH} = P(SOH_{c^N} \leq 0.85)$, i.e., the estimated probability at capacity test c^N that the SOH of the battery is below the threshold $T = 0.85$, c^R is the first capacity test when the decision is to Replace the battery, $p_{c^R}^{SOH} = P(SOH_{c^R} \leq 0.85)$, i.e., the estimated probability at capacity test c^R that the SOH of the battery is below the threshold $T = 0.85$.

VAH#	VAH01	VAH01	VAH05	VAH06	VAH09	VAH10	VAH12	VAH13	VAH15
c^N	8	8	13	10	17	10	11	11	9
$p_{c^N}^{SOH}$	0.044	0.003	0.075	0.008	0.027	0.066	0.009	0.002	0.001
c^R	9	9	14	11	18	11	12	12	10
$p_{c^R}^{SOH}$	0.403	0.902	0.881	0.576	0.750	0.515	0.135	0.135	0.928

VAH#	VAH16	VAH17	VAH20	VAH22	VAH24	VAH25	VAH27	VAH28	VAH30
c^N	7	12	10	8	11	9	7	10	11
$p_{c^N}^{SOH}$	0.001	0.007	0.057	0.035	0.078	0.016	0.066	0.026	0.014
c^R	8	13	11	9	12	10	8	11	12
$p_{c^R}^{SOH}$	0.557	0.905	0.994	0.483	0.702	0.971	0.967	0.241	0.237

5. Conclusions

This paper considers the health monitoring and predictive maintenance planning of batteries for electric vertical take-off and landing (eVTOL) aircraft. The eVTOLs are subject to realistic mission profile, during which the health of the battery is continuously monitored using measurements related to the battery charge and discharge

protocols, the temperature at which the batteries are exposed to, and the eVTOL flight characteristics (e.g., the cruise duration, the power during take-off, cruise and landing). Based on these measurements, features are developed for the estimation of the batteries' State-of-Health. Using the Shapley value, it is shown that the (variance, minimum) of the voltage during take-off and the duration of the CC and CV phases have the highest importance for the SOH estimation. A Convolutional Neural Network with Monte Carlo dropout is employed to estimate the distribution of the SOH of the batteries, i.e., probabilistic SOH prognostics. These prognostics are updated periodically, after every capacity test. The results show that the obtained SOH prognostics are accurate, with the Continuous Ranking Probability Score (CRPS) metric indicating that the estimated SOH distribution is well centered around the true SOH. These probabilistic SOH prognostics are further employed for the maintenance planning of the batteries. Specifically, we determine an optimal time for battery replacement by trading off between the cost of unexpected battery inoperability due to exceeding an End-of-Life threshold, and the cost of replacing the battery early, thus wasting the useful life of the battery. Overall, the paper provides an end-to-end predictive maintenance planning framework, starting from actual measurements obtained by a continuous monitoring of the battery and the mission profiles, to the development of SOH prognostics which are updated periodically, to the planning of the batteries' replacement as a response to the estimated SOH estimated and associated costs.

As future work, we aim to extend our analysis to the development of Remaining-Useful-Life prognostics and to integrated these prognostics into maintenance planning frameworks. For maintenance, we plan to extend the current decision model to consider battery inventory constraints and the availability of slots for maintenance.

Acknowledgements

The research contribution of Zhiguo Zeng is partially supported by Chair of Risk and Resilience of Complex Systems (Chair EDF,SNCF and Orange). This work has been supported as part of France 2030 program ANR-11-IDEX-0003

References

Alba-Maestre, J., Prud'homme van Reine, K., Sinnige, T., Castro, S. 2021. Preliminary propulsion and power system design of a tandem - wing long-range eVTOL aircraft. Applied Sciences, 11083.

Bills, A., Sripad, S., Frederiks, L., Guttenberg, M., Charles, D., Frank, E., Viswanathan, V. 2023. A battery dataset for electric vertical takeoff and landing aircraft. Scientific Data 10, 344.

Caiping, Z., Jiuchun, J., Gao, Y., Zhang, W., Liu, Q., Hu, X. 2017. Charging optimisation in Lithium-ion batteries based on temperature rise and charge time. Applied Energy, 569-577.

de Pater, I., & Mitici, M. (2022). Novel metrics to evaluate probabilistic Remaining Useful Life prognostics with applications to turbofan engines. PHM Society European Conference, 96-109.

Gal, Y., Ghahramani, Z. 2016. Dropout as a Bayesian approximation: Representing model uncertainty in deep learning. International Conference on Machine Learning, 1050-1059.

Granado, L., Ben-Marzouk, M., Saenz, E., Boukal, Y., Juge, S. 2022. Machine learning predictions for lithium-ion battery state-of-health for eVTOL applications. Journal Power Sources, 548:232051.

Huang, S.-C., Tseng, K.-H., Liang, J.-W., Chang, C.-L., Pecht, M. 2017. An online SOC and SOH estimation model for Lithium-ion batteries. Energies, 512.

Li, Y., Berecibar, C., Nanini-Maury, M., Chan, E., van den Bossche, J., van Mierlo, P., Omar, N. 2018. Random forest regression for online capacity estimation of lithium-ion batteries. Applied Energy, 197-210.

Liu, Z., Zhao, J., Wang, H., Yang, C. 2020. A new lithiuim-ion battery SOH estimation method based on an indirect enhanced health indicator and support vector regression in PHMs. Energies, 13:830.

Lundberg, S., & Lee, S.-I. 2017. A unified approach to interpreting predictions. Advances in Neural Information Processing Systems, 30.

Mawonou, K., Eddah, A., Dumur, D., Beauvois, D., Godoy, E. 2021. State-of-health estimators coupled to a random forest approach for lithium-ion battery aging factor ranking. Journal of Power Sources, 229154.

Mitici, M., Hennink, B., Pavel, M., Dong, J. 2023. Prognostics for Lithium-ion batteries for electric Vertical Take-off and Landing aircraft using data-driven machine learning. Energy and AI, 100233.

Polaczyk, N., Enzo, T., Wei, P., Mitici, M. 2019. A review of current technology and research in urban on-demanf air mobility applications. 8th Biennial Autonomous VTOL technical meeting and 6th Annual Electirc VTOL Symposium, 333-343.

Severson, K., Attia, P., Jin, N., Perkins, N., Jiang, B., Yang, Z., Chen, M. 2019. Data-driven prediction of battery cycle life before capacity degradation. Nature Energy, 383-391.

Tian, H., Qin, P., Li, K., Zhao, Z. 2020. A review of the state of health for lithium-ion batteries: Research status and suggestions . Journal of Cleaner Production, 120813.

Wang, B., Lei, Y., Li, N., Yan, T. 2019. Deep separable convolutional network for remaining useful life prediction of machinery. Mechanical Systems and Signal Processing, 106330.

Xiong, R. 2020. Battery management algorithm for electric vehicles. Springer.

Yang, F., Wang, D., Xu, F., Huang, Z., Tsui, K.-L. 2020. Lifespan prediction of Lithium-ion batteries based on various extracted features and gradient boosting regression tree model. Journal of Power Sources, 228654.

Zhang, Y., Xiong, R., He, H., Pecht, M. 2018. Long short-term memory recurrent neural network for remaining useful life prediction of Lithium-ion batteries. IEEE Transactions on Vehicular Technology, 5695-5705.